Journal of Building Engineering 109 (2025) 112963

Contents lists available at ScienceDirect

Journal of Building Engineering

journal homepage: www.elsevier.com/locate/jobe

Assessment of seismic load resistance for STPU-strengthened masonry wall structure

Tae-Hee Lee, Jang-Ho Jay Kim *

School of Civil and Environmental Engineering, Yonsei University, 50 Yonsei-Ro, Seodaemun-Gu, Seoul, 03722, Republic of Korea

ARTICLE INFO

Keywords:
Aged structures
Masonry structure
STPU
Retrofitting
Shaking table test

ABSTRACT

As seismic activity in Korea increases, concerns over aging masonry structures grow. By 2030, over 62 % of South Korea's buildings will be more than 30 years old, with masonry structures are a dominant structural type in older structures. Due to the low tensile strength of mortar, masonry buildings are highly vulnerable to seismic loads, requiring effective retrofitting and strengthening solutions. This study evaluates the seismic strengthening effects of stiff-type polyurea (STPU) and glass fiber-strengthened polymer (GFRP) on masonry walls through shaking table tests. Three strengthening types were tested: non-strengthened (MWN), STPU-strengthened (MWP2), and hybrid GFRP + STPU-strengthened (MWPF5) specimens. The results show that MWP2 resisted up to 0.8 g PGA, twice the capacity of the non-strengthened specimens (0.4g–0.5 g PGA). The hybrid MWPF5 exhibited the highest seismic resistance, withstanding up to 1.0 g PGA, but also showed increased acceleration, indicating improved structural stiffness and potential brittle failure. The findings confirm that STPU significantly enhances ductility, energy absorption, and seismic resistance, while GFRP further improves structural seismic performance. These strengthening materials offer effective and practical retrofitting solutions for aging masonry structures vulnerable to earthquakes. Further details on the experiments and results are discussed in the paper.

1. Introduction

The number of earthquakes in Korea has increased over the past few years. For example, 93 earthquakes greater than 2.0 on the Richter scale occurred in 2013—twice as many as the annual mean number of earthquakes (44.5) that occurred in Korea from 1999 to 2012 [1,2]. Furthermore, earthquakes exceeding 5.1 and 5.0 in magnitude on the Richter scale occurred on the west-central and southeastern seashore of the Korean Peninsula, respectively [3,4]. As of 2020, 38.8 % of South Korea's buildings (7.27 million) were over 30 years old; by 2030, this is predicted to soar to 62 %. In South Korea, buildings constructed before the late 1980s were largely designed not following comprehensive seismic codes. Although modern seismic design standards are now well-established, the first mandatory seismic design code was only introduced in 1988 [5]. To address the aging of structures in South Korea, preemptive maintenance plans are urgently needed. Particularly in Seoul (in South Korea), masonry construction is the predominant architectural form in 60.3 % of structures over 30 years old [6]. The strength of mortar significantly influences the structural performance of masonry constructions. Mortar is a material with very low tensile strength; hence, masonry structures are more vulnerable to seismic loads than RC structures [7,8]. Therefore, research on repair and strengthening materials and methods for application to older masonry

* Corresponding author.
E-mail address: jjhkim@yonsei.ac.kr (J.-H.J. Kim).

https://doi.org/10.1016/j.jobe.2025.112963
Received 25 November 2024; Received in revised form 28 February 2025; Accepted 20 May 2025
Available online 27 May 2025

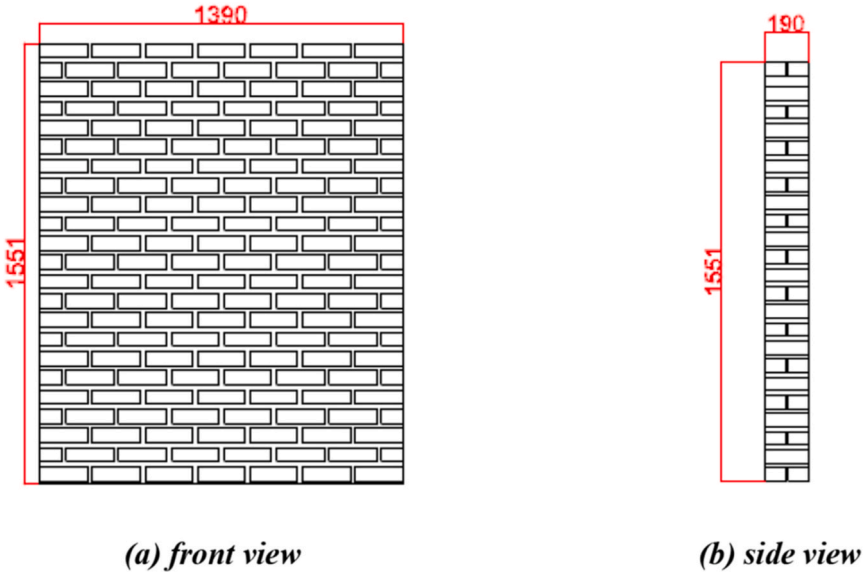

Fig. 1. Masonry wall specimen for shaking table test.

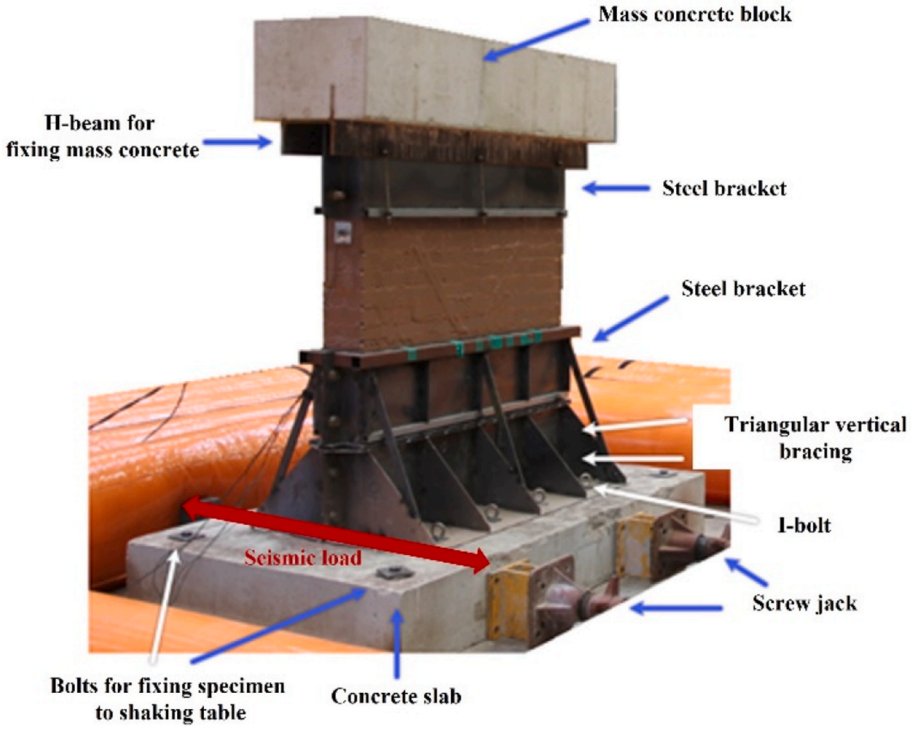

Fig. 2. Shaking table test specimen details.

structures to make these structures more earthquake-resistant has been garnering increasing interest [9].

Various retrofitting techniques have been developed to enhance the seismic resistance of masonry walls, each with advantages and limitations. One of the most studied retrofitting methods is fiber-reinforced polymer (FRP) strengthening, which enhances the tensile capacity and ductility of masonry walls [10–13]. However, FRP systems depend on epoxy adhesives, which degrade over time due to environmental exposure, leading to a reduction in bond strength and effectiveness [14–16]. To overcome the limitations of FRP, researchers have investigated fabric-reinforced cementitious matrix (FRCM) systems, where fiber grids are embedded in mortar layers [17,18]. Recent research by Mercuri et al. (2024) explored the effectiveness of basalt and glass chopped fiber mortar for masonry

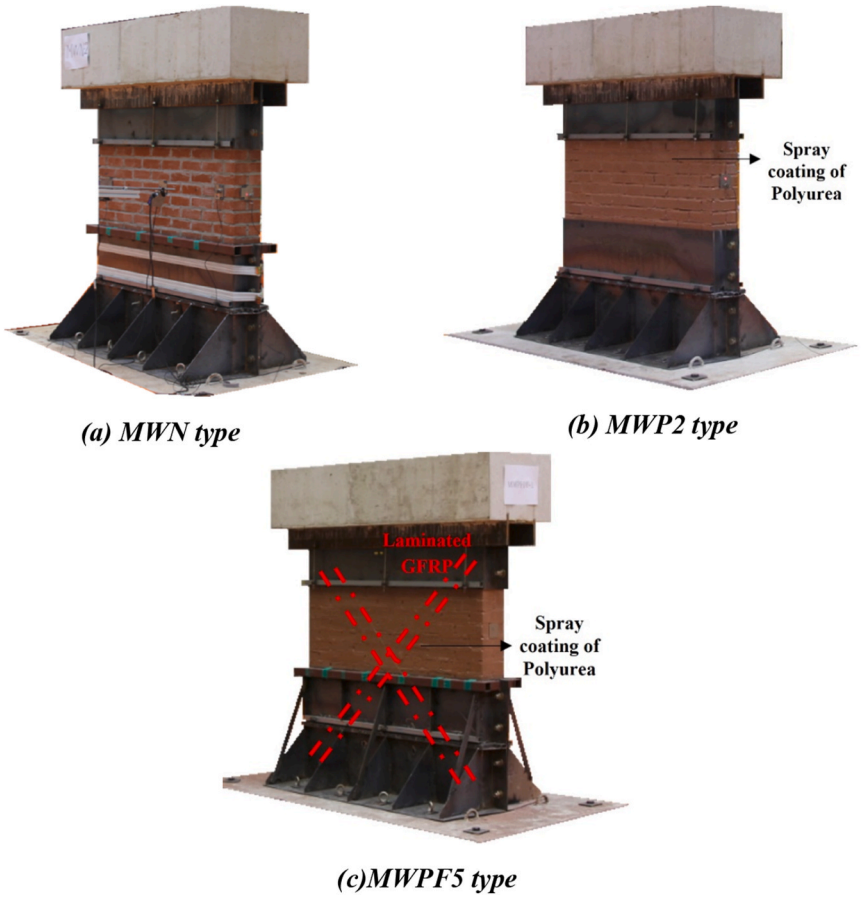

Fig. 3. Shaking table test specimen type.

reinforcement [18]. This study emphasized the role of bed joints and coating reinforcements in improving structural integrity under seismic loads [18]. This suggests that fiber-based mortar systems can be a promising alternative to conventional FRP, but further evaluation of their long-term durability and application feasibility is needed. Methods for strengthening structures include increasing the cross-sectional area with reinforced concrete or steel bracing, but these methods are expensive and time-consuming [19–21]. Therefore, there is a critical need for a retrofitting method that offers ease of application, enhanced durability, and cost-effectiveness while addressing the limitations associated with conventional strengthening methods.

Polyurea (PU) is highly beneficial for retrofitting and strengthening aging structures due to its affordability, high durability, high ductility, short curing time, and suitability for application in wrapping forms on existing structures [22–27]. Lee et al. (2022) developed stiff-type PU (STPU) by modifying the chemical properties of existing PU [28]. The tensile strength, percent of elongation, and elastic modulus of STPU are 28 MPa, 250 %, and 112 MPa, respectively, while those of general PU are 24 MPa, 310 %, and 108 MPa [28]. STPU has a higher tensile strength and lower elongation percentage than existing PU, so it is expected to have a higher energy absorption, load-carrying capacity, and confinement effect when applied to structures [29]. In this study, STPU was selected as the strengthening material for masonry walls under seismic load. This study aimed to simulate extreme conditions with the development of a new strengthening material, STPU, such as the application of seismic loads to a masonry wall in the out-of-plane direction and mass concrete on top of the specimen, to assess its seismic load resistance. Three types of specimens (non-strengthened, STPU-strengthened, and STPU + GFRP-strengthened) were used for shaking table test to evaluate their seismic resistance.

2. Shaking table test specimens and set-up

2.1. Shaking table test specimens

The masonry wall specimen used in the shaking-table test had dimensions of 1390 × 1551 × 190 mm and weighed 700 kg as shown in Fig. 1. The clay brick dimensions were 190 × 57 × 90 mm and comprised 23 layers with 10 mm mortar joints. The compressive strengths of clay brick and mortar are 25 and 30 MPa, respectively. To connect the specimen to the shaking table, the masonry wall was placed on top of a 2300 × 300 × 1500 mm concrete slab. A 1750 × 370 × 540 mm concrete block was placed on top of the masonry wall to apply inertial loads during the test. The bottom 880 mm and top 440 mm of the masonry wall were restrained using steel

Table 1
Strengthening types.

Wall denomination	Strengthened method	Size (mm)
MWN	Non-strengthened	1390 × 1551 × 190
MWP2	2 mm layer of polyurea sprayed onto the surfaces	1390 × 1551 × 190
MWPF5	GRFP laminated in an X pattern on both the front and back surfaces, and a 2 mm layer of polyurea is sprayed onto the surfaces	1390 × 1551 × 190

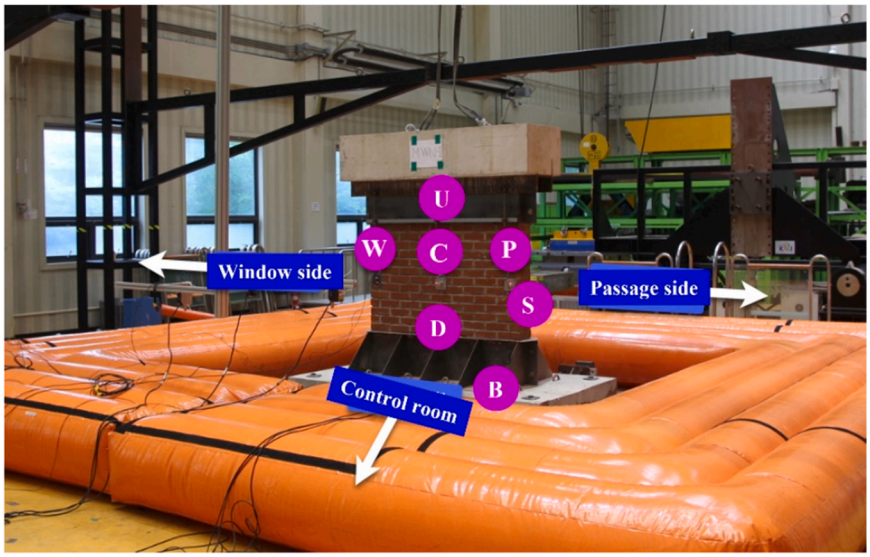

Fig. 4. Shaking table test sensor placement.

Table 2
Sensor placement labeling (in Fig. 4).

Y	Sensor placement
B	Concrete slab (Base)
U	Specimen upward
C	Specimen center
D	Specimen downward
S	Specimen side
W	Window side
P	Passage side

brackets to ensure that failure occurred at the center of the specimen. Fig. 2 shows the details of the masonry wall specimen installed on the shaking table. The seismic load was applied in the lateral direction, as shown in Fig. 2. Three types of specimens were made as shown in Fig. 3. And Table 1 summarizes the strengthening types applied to the masonry wall specimens used in this study.

The denomination system for the masonry wall specimens is as follows. "MW" represents the masonry wall, followed by a letter indicating the strengthening method. "N" denotes a non-strengthened specimen, while "P2" denotes a 2 mm STPU-strengthened specimen. Additionally, "PF5" refers to specimens strengthened with both 50 mm width laminated GFRP and STPU on the entire surface. The number after the hyphen represents the specimen number.

A total of seven specimens were prepared: three non-strengthened masonry wall specimens (MWN), two STPU- strengthened specimens covering the entire surface (MWP2), and two specimens strengthened with both laminated GFRP and STPU (MWPF5). The GFRP used in the strengthening has a tensile strength of 900 MPa and an elastic modulus of 45 GPa.

2.2. Shaking table test set-up

The denomination system for the sensors used in the shaking-table test is structured as follows. The first letter represents the sensor type, where "A" indicates an accelerometer and "L" indicates a laser LVDT. The second letter denotes the sensor attachment area, which

Table 3
Maximum values obtained by sensors in MWN specimen.

PGA.	Spcm.								
	MWN-1		MWN-2		MWN-3				
	ABK	ACK	ACK	LC	ACD	ACK	LU	LC	LD
0.1 g	−0.09	−0.08	−0.08	−7.46	−0.13	−0.13	8.19	8.12	8.04
0.2 g	−0.22	0.29	−0.18	−15.77	−0.28	−0.29	−15.39	15.14	−15.24
0.3 g	−0.31	0.47	−0.26	23.89	−0.32	−0.33	24.88	24.53	24.30
0.4 g	−0.43	−0.31	0.31	−33.45	−0.57	−0.55	53.36	34.97	31.34
0.5 g			−0.94	44.91					

*Accelerometer unit: g, LVDT unit: mm.

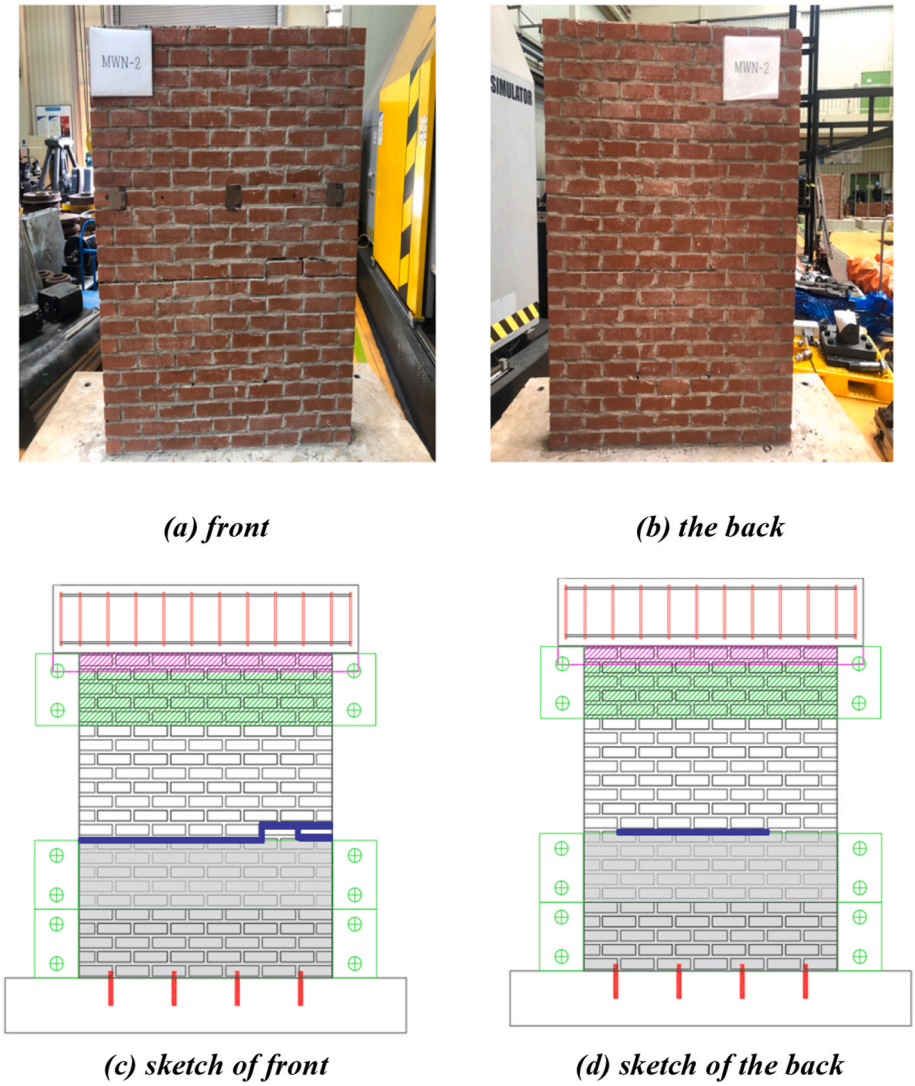

Fig. 8. Crack pattern in MWN-2 specimen.

corresponds to the locations specified in Fig. 4 and Table 2. The third letter identifies the brand of the accelerometer, with "D" referring to a Dytran accelerometer (ICPE type) and "K" referring to a Kyowa accelerometer (Bridge type). The third letter was not used for LVDT and was only applied to accelerometers (see Table 2).

During the shaking-table test, the El-Centro earthquake wave was selected as the input ground motion. The peak ground acceleration (PGA) was incrementally scaled from 0.1 g to 1.0 g in 0.1 g step to simulate increasing seismic intensity and capture the

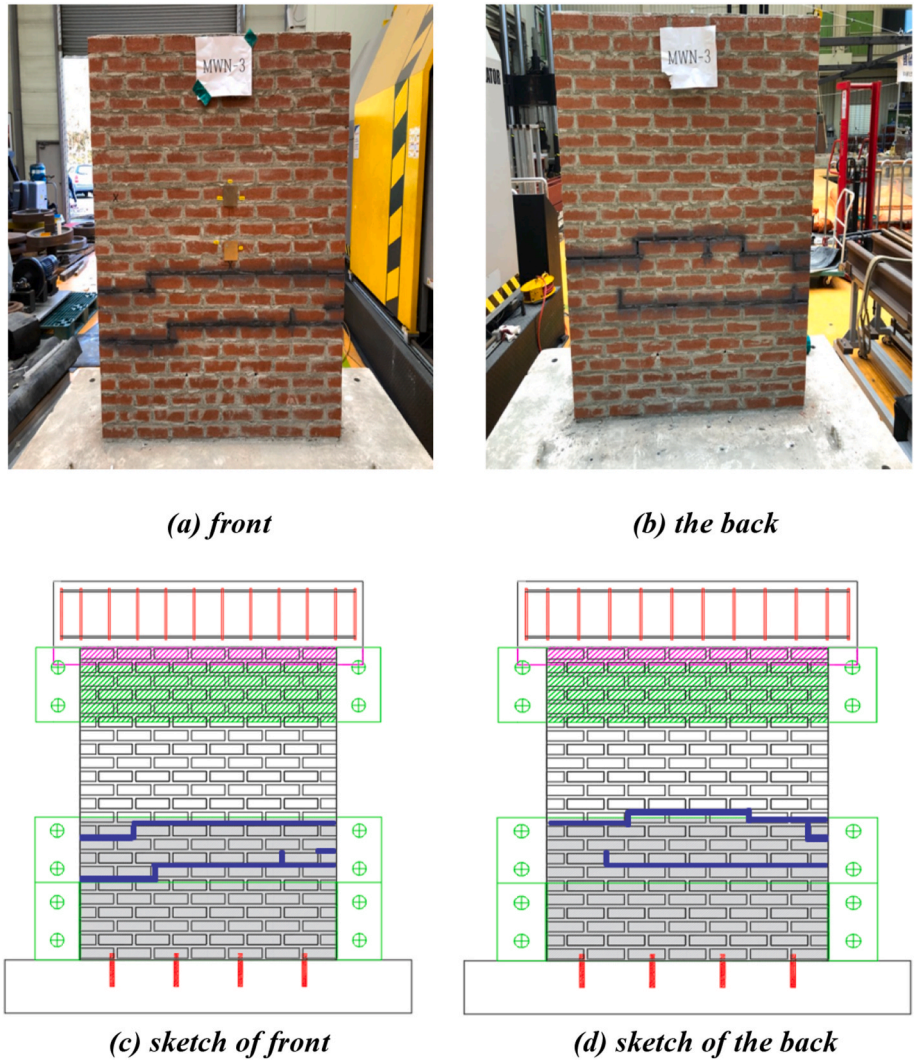

Fig. 9. Crack pattern in MWN-3 specimen.

Table 4
Maximum values obtained by sensors in MWP2 specimen.

PGA.	Spcm.						
	MWP2-1			MWP2-2			
	ABK	ACK	LC	ABK	ACK	LU	LC
0.1 g	−0.09	−0.08	−7.50	−0.08	−0.11	8.28	7.84
0.2 g	−0.22	−0.14	−15.29	−0.14	−0.2	15.48	14.97
0.3 g	−0.30	−0.18	25.25	−0.21	−0.27	25.21	24.46
0.4 g	−0.43	−0.26	32.15	−0.44	−0.51	−32.40	−31.60
0.5 g	−0.63	0.58	47.69	−0.50	0.57	−42.51	−40.02
0.6 g	−0.72	0.73	49.95	−0.65	−0.86	49.29	47.68
0.7 g	−0.81	0.88	58.78	−0.71	−1.30	59.89	57.26
0.8 g				−0.86	1.04	80.20	65.49

*Accelerometer unit: g, LVDT unit: mm.

progressive failure mechanisms of the walls. Since STPU was newly developed for structural seismic strengthening material, the test was designed to simulate extreme conditions by applying the seismic load in the out-of-plane direction. This is a critical failure mode for masonry walls, as they are particularly vulnerable to out-of-plane forces due to their low tensile strength. The test was terminated when structural failure occurred, ensuring that the ultimate capacity of each specimen was identified.

Table 5
Peak value comparison between MWN and MWP2 at PGA 0.3 g.

	ACK (g)	LC (mm)	Average		Ratio	
			ACK (g)	LC (mm)	ACK	LC
MWN-2	0.26	23.89	0.295	24.21	1	1
MWN-3	0.33	24.53				
MWP2-1	0.18	25.25	0.225	24.86	0.76	1.03
MWP2-2	0.27	24.46				

(a) shaking table test photo

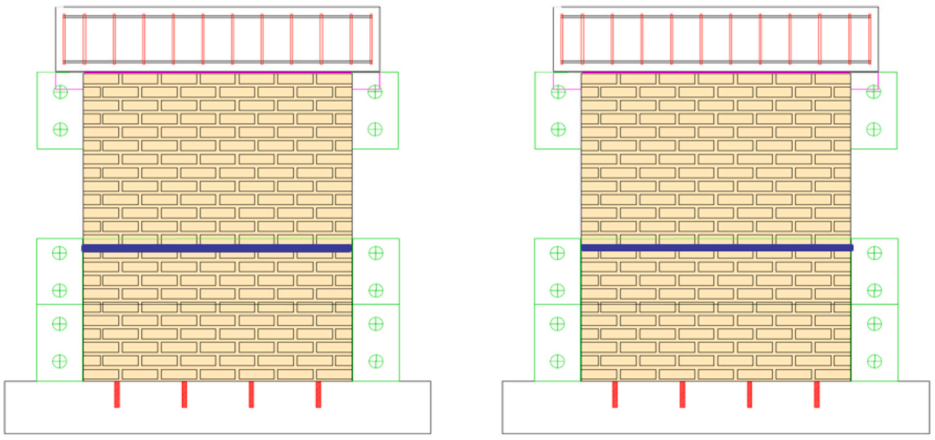

(b) sketch of front *(c) sketch of the back*

Fig. 12. Crack patterns in MWP2-1 specimen.

3. Shaking table test result

3.1. MWN specimen test result

The absolute maximum measurement values for each sensor of the MWN specimen are listed in Table 3. The MWN-1 specimen was

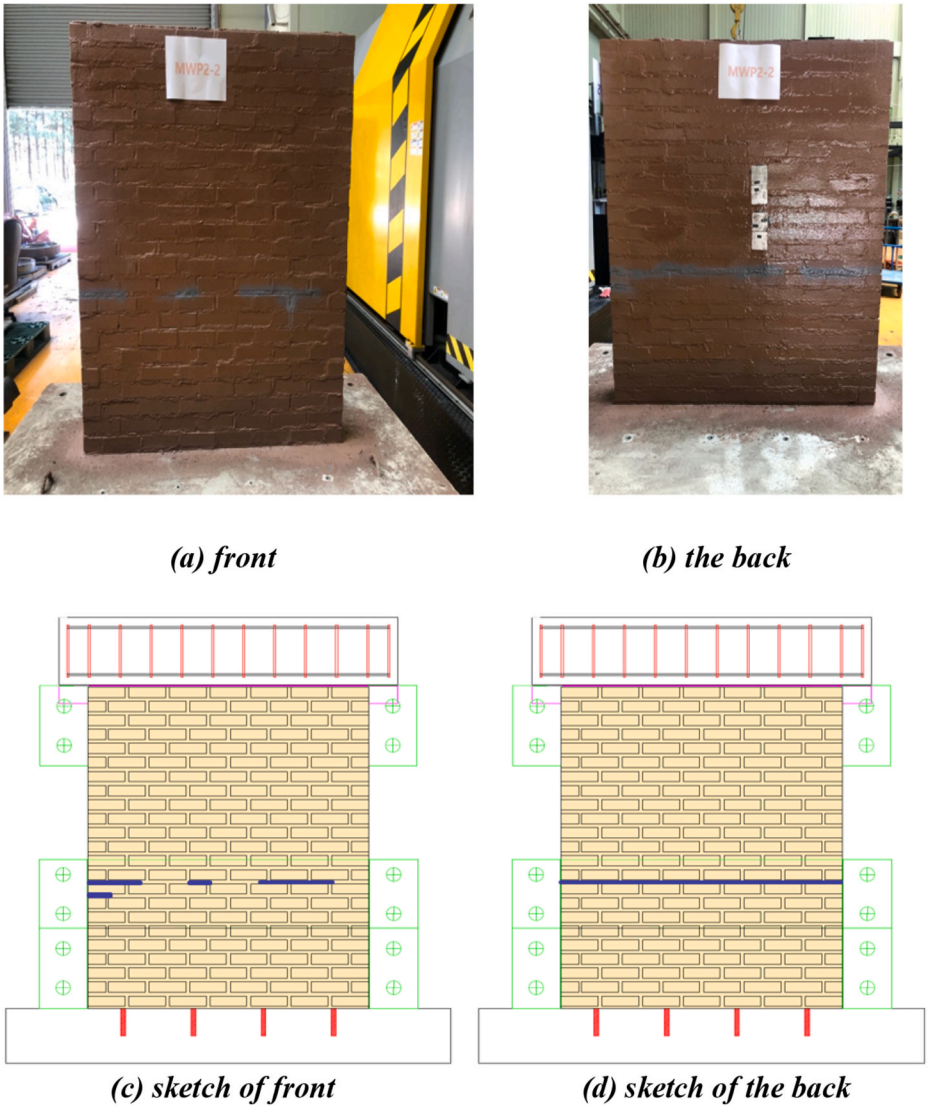

Fig. 13. Crack patterns in MWP2-2 specimen.

Table 6
Maximum values obtained by sensors in MWPF5 specimens.

PGA.	Spcm.									
	MWPF5-1					MWPF5-2				
	ABK (g)	ACK (g)	LU (mm)	LC (mm)	LD (mm)	ABK (g)	ACK (g)	LU (mm)	LC (mm)	LD (mm)
0.1 g	−0.14	−0.11	−7.75	7.51	7.61	−0.14	−0.13	−8.01	−7.73	−7.82
0.2 g	−0.26	−0.43	−15.85	−15.54	−15.92	−0.23	−0.29	−16.18	−19.44	−15.76
0.3 g	−0.32	−0.41	24.17	24.05	23.76	−0.34	−0.31	26.24	25.50	25.68
0.4 g	−0.43	−0.61	−32.84	−32.52	−31.72	−0.43	−0.54	−34.74	−34.27	−33.68
0.5 g	−0.52	−0.63	−41.93	40.81	39.68	−0.57	−0.71	47.94	43.41	45.16
0.6 g	−0.68	−1.04	51.65	48.62	46.96	−0.75	−1.22	−52.83	−48.68	−49.80
0.7 g	−0.76	−0.81	63.48	56.47	54.00	−0.80	1.00	63.66	59.42	60.68
0.8 g	−0.84	−1.18	83.85	72.39	67.83	−0.92	1.11	74.07	64.63	67.04
0.9 g	−1.00	−1.82	−103.53	85.37	−79.03	−1.05	−1.15	−106.68	−90.43	−100.67
1.0 g	−1.01	1.80	−133.04	84.97	−94.48	–	–	–	–	–

Table 7
Mean value comparison among three types of specimens.

PGA.	Spcm.									
	ACK (g)			Ratio (MWPF5/ MWN)	Ratio (MWPF5/ MWP2)	LC (mm)			Ratio (MWPF5/ MWN)	Ratio (MWPF5/ MWP2)
	MWN	MWP2	MWPF5			MWN	MWP2	MWPF5		
0.1 g	0.10	0.10	0.12	1.20	1.20	7.80	7.67	7.62	0.97	0.99
0.2 g	0.23	0.17	0.36	1.57	2.12	15.46	15.13	17.49	1.13	1.16
0.3 g	0.30	0.23	0.36	1.20	1.57	24.21	24.86	24.78	1.02	1.00
0.4 g	0.44	0.39	0.58	1.32	1.49	34.21	31.88	33.40	0.98	1.05
0.5 g	0.94 (Failure)	0.58	0.67	0.71	1.16	44.91 (Failure)	43.86	42.11	0.94	0.96
0.6 g	–	0.79	1.13	–	1.43	–	48.82	48.65	–	1.00
0.7 g	–	1.09	0.91	–	0.83	–	59.34	57.95	–	0.98
0.8 g	–	1.04 (Failure)	1.15	–	1.11	–	80.20 (Failure)	68.51	–	0.85

subjected to a preliminary test to improve the reliability of the shaking-table test before the actual test. The lower MWN-1 fixed bracket was installed with only one tier (440 mm), and the laser LVDT was installed at the center and on the left and right sides of the wall. However, data could not be acquired due to a data logger malfunction. Figs. 5–7 (in Appendix A.) provide graphs of the primary sensor measurements for each specimen, which are separated into pre- and post-failure PGAs, whereas Figs. 8 and 9 depict the crack patterns for the MWN-2 and MWN-3 specimens after the shaking table test. Installing a fixed steel bracket on MWN-2 and MWN-3 caused damage in the central region, to emphasize observation of data from the central region. For MWN-1, failure occurred at 0.4 g; however, for MWN-2, failure did not occur until 0.4 g, although cracks appeared, and it was determined that MWN-2 was failed when the cracks expanded at 0.5 g. As observed in Table 3 and Fig. 7 (in Appendix A.), MWN-3 was failed at 0.4 g when the values of the center displacement (LC) and that of the upper displacement (LU) differed markedly. The acceleration data in Figs. 5–7 (in Appendix A.) reveals that, before failure progressed, the amplitude of the acceleration graph in the central area decreased after 5 s. However, this phenomenon was less frequent as failure progressed. Presumably, the acceleration increases due to the vibration induced by the failure, as the effect of acceleration reduction by damping decreases after failure. Figs. 8 and 9 show that most of the mortar cracks occurred at the top of the lower fixed bracket and advanced downward.

3.2. MWP2 specimen test result

The absolute maximum values for each sensor of the MWP2 specimen are listed in Table 4, and the comparison of peak values of ACK and LC for MWN and MWP2 specimen at 0.3 g PGA are listed in Table 5. The graphs for each main sensor in Figs. 10 and 11 (in Appendix A.) show the PGA before failure and the PGA after failure. MWP2-1 failed at 0.8 g, and as shown in Fig. 12 (a), the specimen was separated into two parts for the torn STPU coating. Failure was observed at 0.7 g. The difference in MWP2-2 between the LC and the LU was minimal until 0.7 g, but at 0.8 g, the difference was 14.7 mm, and failure occurred. Figs. 12 and 13 illustrate the crack pattern of the MWP2 specimens; cracks were observed near the top of the lower fixing bracket. In specimen MWP2-1, the STPU tore apart, causing the specimen to split into two parts. This phenomenon is attributed to the concentration of load at the lower fixing bracket, which restrained the bottom part. Presumably, if there were no restrained areas on the surface when strengthening the structure with STPU, the STPU would not tear.

In comparing the average experimental values between specimens MWN and MWP2, failure was observed when the seismic loads were 0.4g–0.5 g and 0.7g–0.8 g, respectively. Thus, the seismic load resistance of specimen MWP2 was 0.2g–0.4 g higher than that of specimen MWN. The central acceleration did not differ between specimens MWN and MWP2 when the PGA was 0.1 g; however, it decreased by 11–48 % when the seismic load was 0.2g–0.5 g. The displacement value of MWP2 was 2–7 % lower than that of MWN except when the PGA was 0.3 g. Strengthening with STPU increased the ductility of the structure, resulting in higher seismic load resistance. As ductility increased, a rise in energy absorption and a reduction in structural acceleration were observed.

3.3. MWPF5 specimen test result

The absolute maximum values for each sensor of the MWPF5 specimen are listed in Table 6, and the comparison of the mean values of ACK and LC for specimens MWN, MWP2, and MWPF5 are shown in Table 7 and Fig. 14. The graphs for each main sensor in Figs. 15 and 16 (in Appendix A.) show the PGA before failure and the PGA after failure. The structure of specimen MWPF5-1 did not fail during the test until the PGA was 1.0 g. However, as listed in Table 6, when the difference between the LC and LU values of MWPF5-1 exceeds 10 mm when the load is 0.8 g, cracks are assumed to occur at 0.7g–0.8 g. Figs. 15 and 16 (in Appendix A.) show that after the failure of specimens MWPF5-1 and MWPF5-2, the amplitude of the LU graph increases by more than 20 mm compared to that of the LU graph before the specimens were failed. When MWPF5-2 was failed at 0.9 g, noise occurred in the ACK data due to the central part of the specimen being damaged. The maximum values observed before 20 s when the specimen was not failed are summarized in Table 6. Figs. 17 and 18 illustrate the crack pattern of the MWPF5 specimens. For specimen MWPF5-2, at 0.8 g, the difference between the maximum values of LC and LU is 9.56 mm, which is approximately 10 mm. Thus, specimen MWPF5-2 is deduced to have also cracked

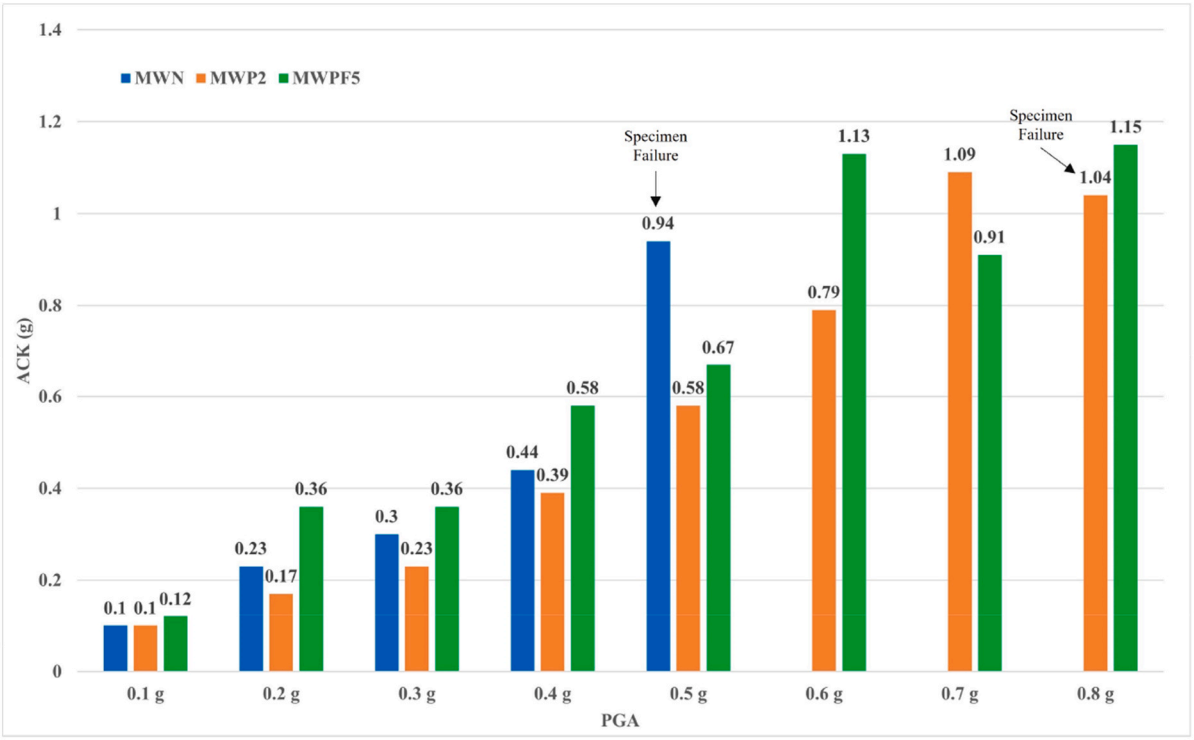

(a) ACK

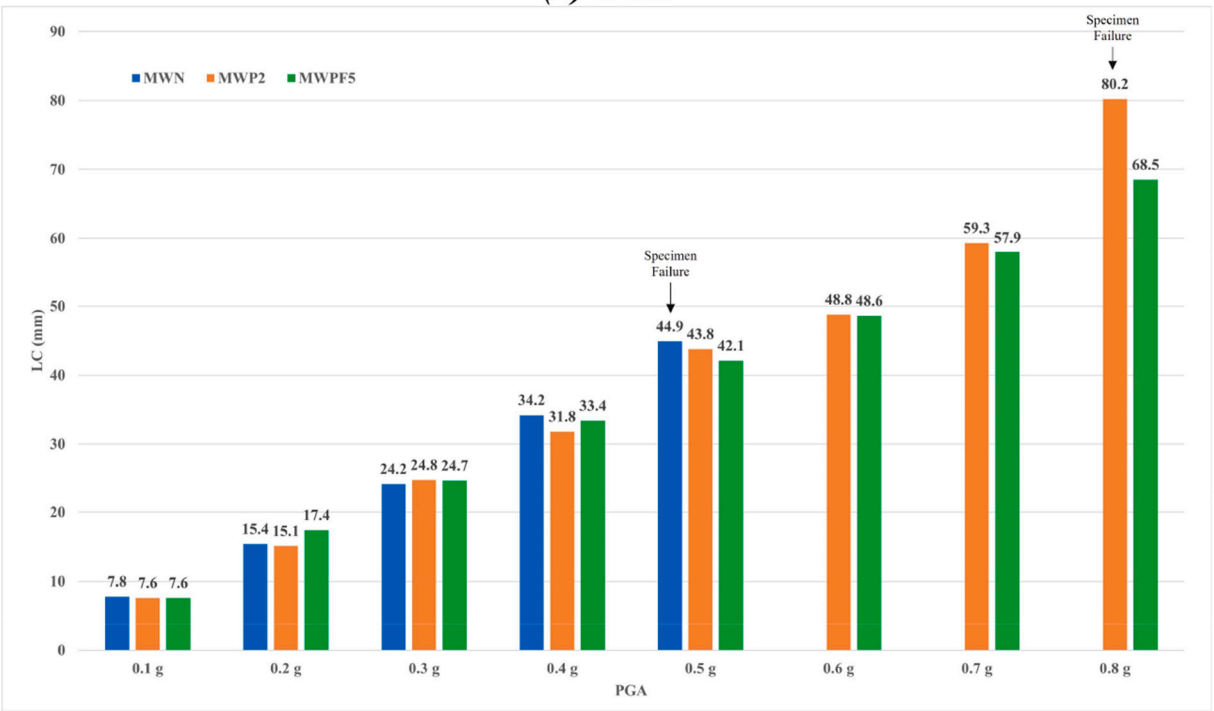

(b) LC

Fig. 14. Mean value comparison among three types of specimens.

at 0.7g–0.8 g. Regarding the crack pattern of MWPF5-1 shown in Fig. 17, cracks are observed near the top of the lower fixing bracket. Regarding the crack pattern of MWPF5-2 shown in Fig. 18, cracks are also observed near the top of the lower fixing bracket and near the laminated GFRP. The seismic load resistance values of specimen MWPF5 are 0.4g–0.6 g and 0.1g–0.3 g higher than those of MWN

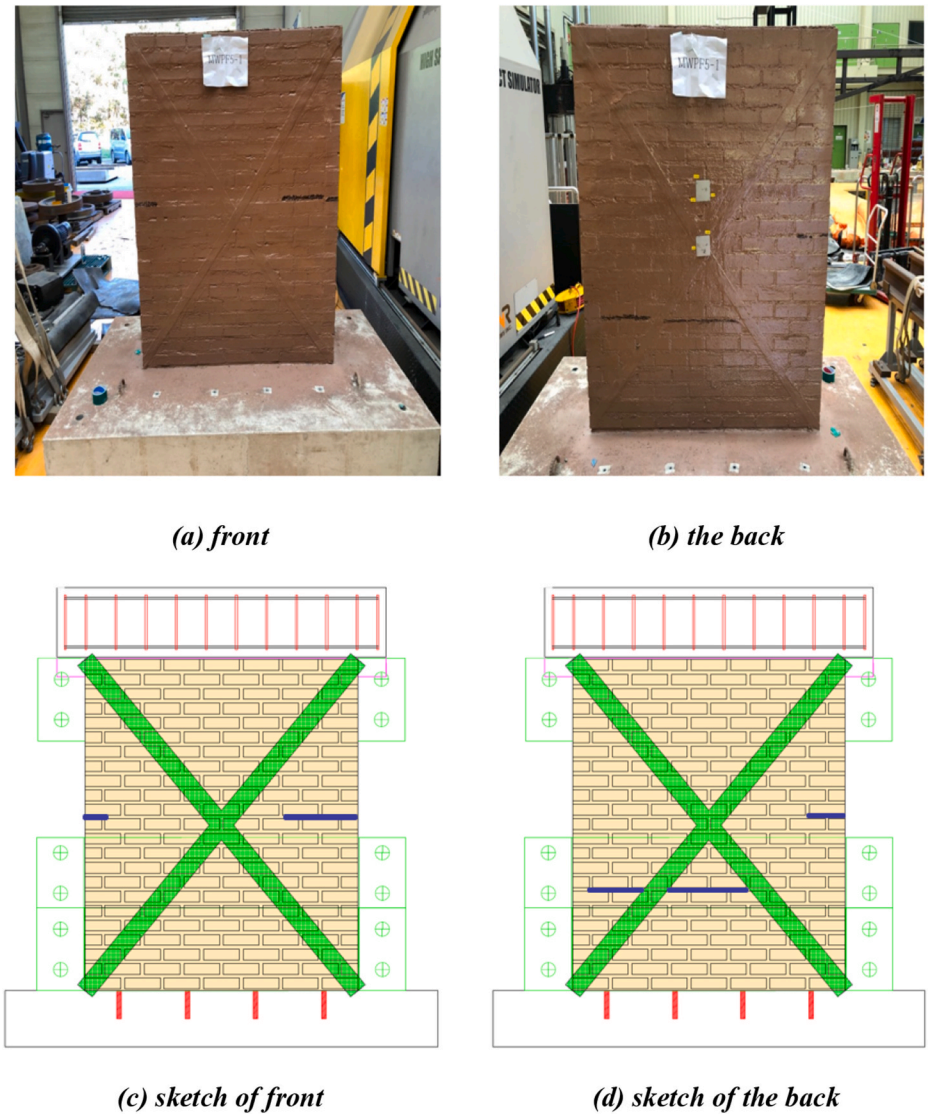

Fig. 17. Crack pattern in MWPF5-1 specimen.

and MWP2, respectively. The ACK data summarized in Table 7 indicate that specimen MWPF5 has acceleration values higher than those of specimen MWN except when the PGA is 0.5 g and higher than those of MWP2 except when the PGA is 0.7 g. The LC values in Table 7 indicate that the displacement values of specimen MWPF5 are similar to those of specimens MWN and MWP2 for each load except when MWP2 is failed at 0.8 g. Due to the stiffness of GFRP being higher than that of STPU, strengthening with GFRP + STPU resulted in a higher acceleration response under seismic loads than strengthening with STPU alone. These results reveal that when STPU and GFRP are used together as strengthening material, the strengthening effect of GFRP, which is stiffer than that of STPU, is more pronounced. Specimens strengthened with GFRP + STPU exhibited higher seismic load resistance than those strengthened with STPU alone, but they also exhibited a higher acceleration response, suggesting an improved structural stiffness and a potential risk of brittle failure when the specimen fails.

In the shaking table test, the displacement of each specimen was measured using a laser displacement meter. Measurement was conducted outside the shaking table in anticipation of specimen collapse. The displacement of the shaking table and the displacement of the specimen due to the seismic load were added. Accordingly, the inherent displacement of the specimen due to seismic load can be derived from the relative displacement, which is obtained by subtracting the displacement of the shaking table from that of the specimen. The maximum relative displacement values comparison among specimens MWN-3, MWP2-2, MWPF5-1, and MWPF5-2 are summarized in Table 8 and Fig. 19. The displacement data relative to these specimens could be collected from the shaking table tests. The LU value of specimen MWN-3 gradually increased until the load was 0.3 g. A sharp increase was then observed at 0.4 g, and the specimen was failed. The LU value of specimen MWP2-2 gradually increased to 1.5 mm at 0.4 g; then, it approximately doubled to 3.06 mm at 0.5 g. However, because the specimen displacement (i.e., 3 mm) was relatively small, microcracks were deduced to occur at

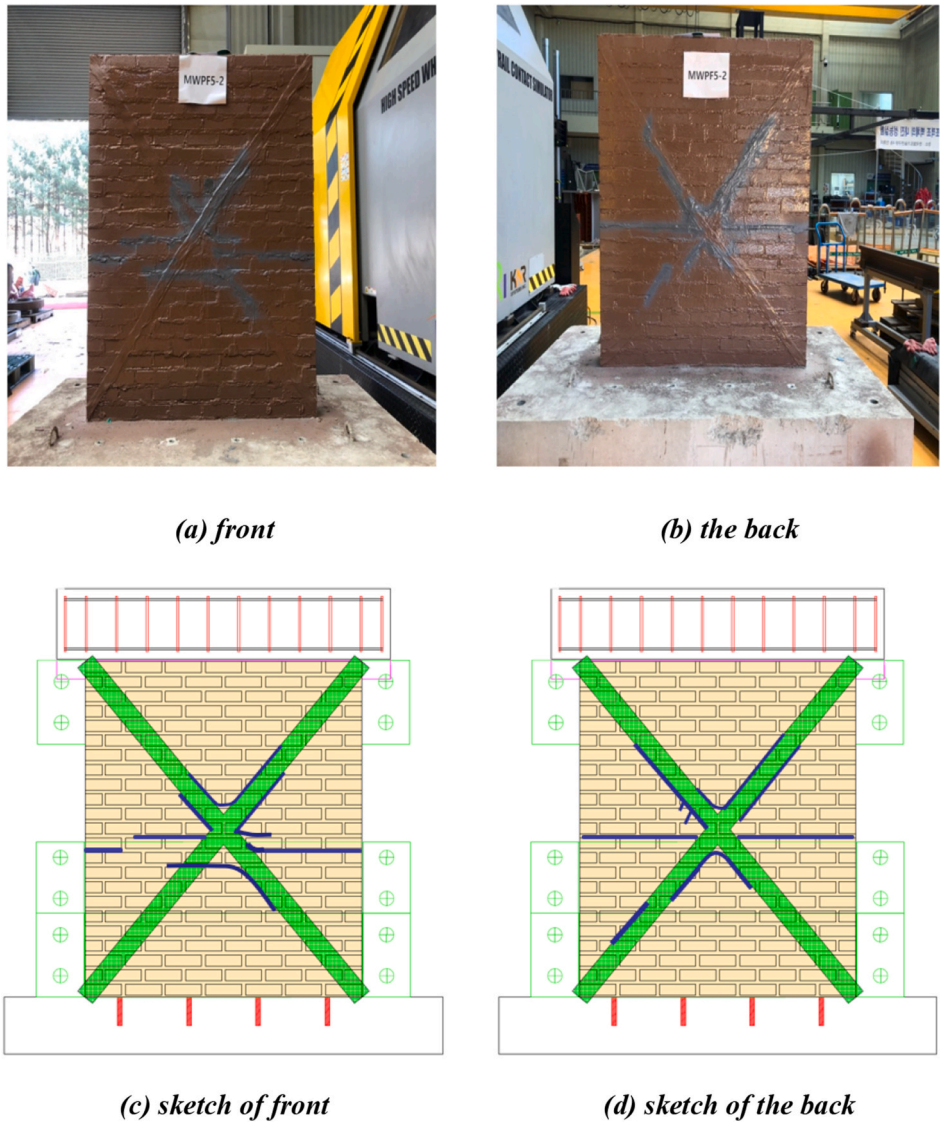

Fig. 18. Crack pattern in MWPF5-2 specimen.

Table 8
Maximum relative displacement results.

PGA.	Spcm.							
	MWN-3		MWP2-2		MWPF5-1		MWPF5-2	
	LU (mm)	LC (mm)	LU (mm)	LC (mm)	LU (mm)	LC (mm)	LU (mm)	LC (mm)
0.1 g	0.37	0.20	0.26	0.19	−0.81	−0.40	−0.27	0.19
0.2 g	−1.06	0.31	−0.57	−0.28	−1.05	0.88	0.63	0.49
0.3 g	−1.92	0.51	−0.75	0.32	−2.45	−1.15	−1.77	1.21
0.4 g	40.72 (Failure)	14.14 (Failure)	−1.50	0.58	−4.06	−1.80	−3.38	2.40
0.5 g	–	–	−3.06	1.26	−5.26	−2.21	−4.12	2.26
0.6 g	–	–	−3.16	1.30	−10.64	−4.37	−4.36	−5.02
0.7 g	–	–	−3.88	−1.67	−12.61	−5.31	−4.70	−5.36
0.8 g	–	–	13.80 (Failure)	−6.43 (Failure)	27.01	−8.83	7.28	−8.64
0.9 g	–	–	–	–	51.16	17.77	−53.21 (Failure)	−29.12 (Failure)
1.0 g	–	–	–	–	67.08 (Failure)	30.53 (Failure)	–	–

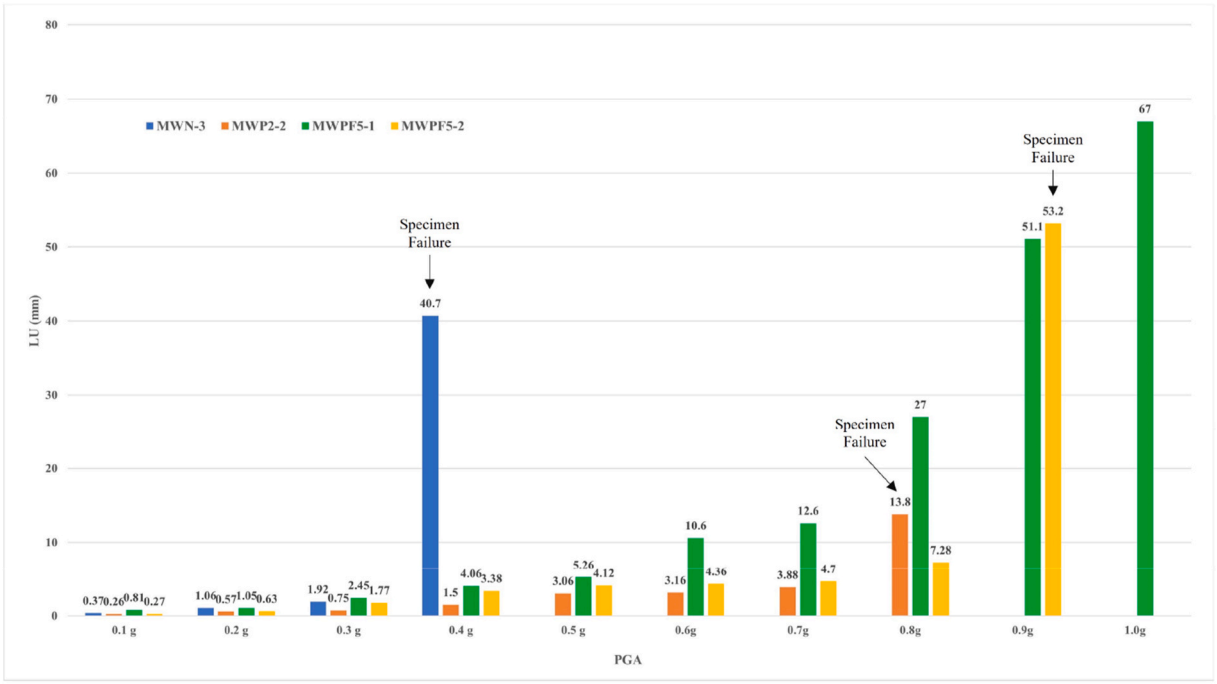

Fig. 19. Maximum relative displacement results (absolute value).

0.4g–0.5 g. The LU value of specimen MWP2-2 gradually increased when the acceleration was 0.5g–0.7 g and finally increased to 13.8 mm at 0.8 g before the specimen was failed. This value is approximately 3.56 times higher than that at 0.7 g. The LU and LC values of specimen MWPF5-1 gradually increased at 0.5 g. The LU value at 0.6 g then increased to approximately double that at 0.5 g. Subsequently, the LU value increased approximately 1.9 times at 0.8 g compared with that at 0.7 g. Specimen MWPF5-1 reached higher relative displacement values of LU than specimens MWN-3 and MWP2-2 at the same load. In specimen MWPF5-1, cracks occurred in the bricks and mortar at 0.4g–0.8 g. However, with STPU and GFRP as strengthening material, ductility was achieved, preventing the

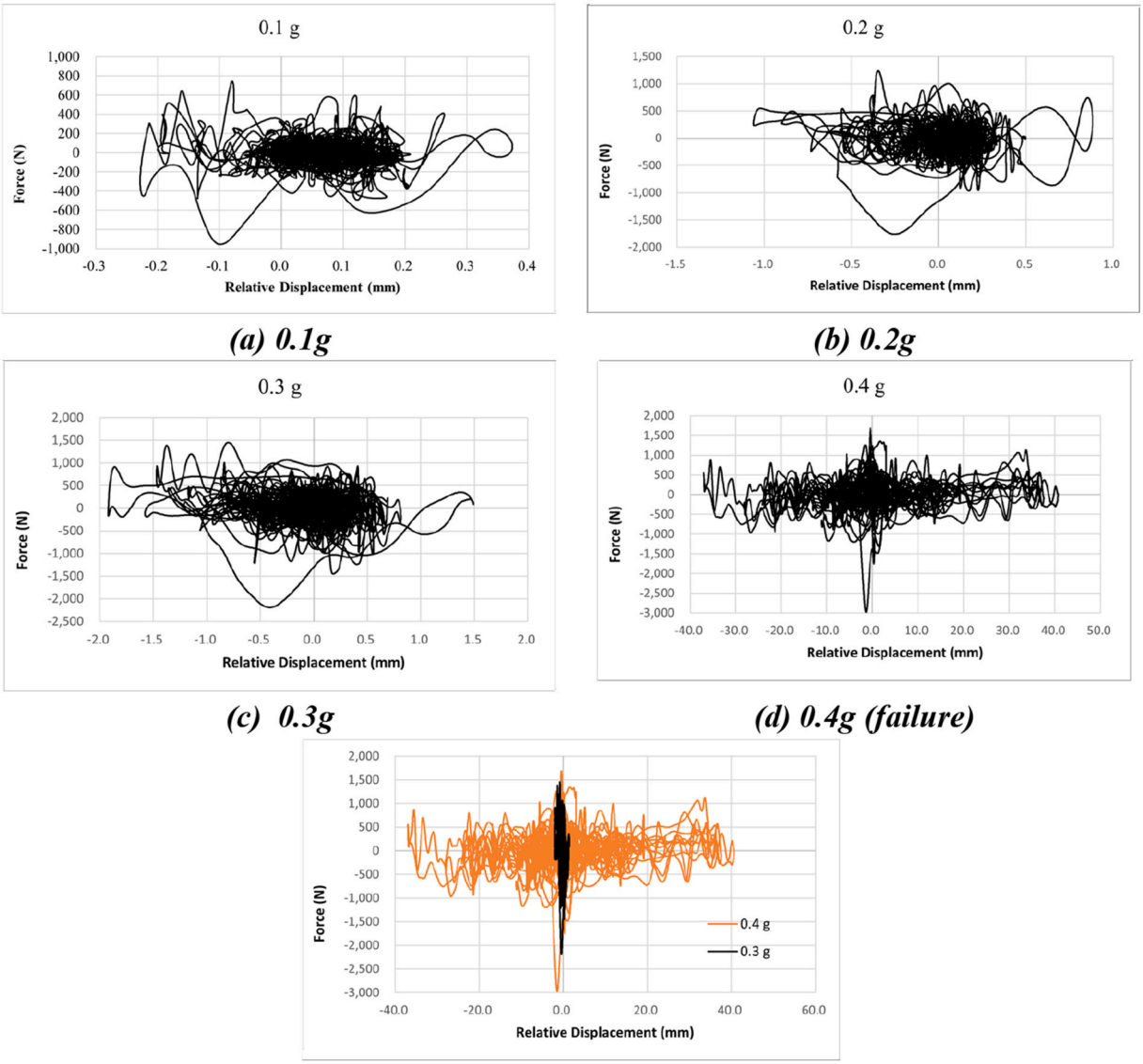

Fig. 20. MWN-3 specimen hysteretic curves.

wall from collapsing. Specimen MWPF5-1 exhibited considerable displacement with an LU value of 51.06 mm at 0.9 g, and the damage to the wall was marked. However, the wall was not failed; presumably, debonding did not occur between the GFRP and the masonry wall. The LU value of specimen MWPF5-2 gradually increased until the load was 0.8 g. Then, it increased to −53.21 mm at 0.9 g, and failure occurred; this LU value was approximately 7.3 times greater than that at 0.8 g. In specimen MWPF5-2, the LC value was observed to be higher than the LU value after the acceleration reached 0.6 g. However, the value was incorrect because of noise and errors during measurement. Based on relative displacement, both specimens MWP2 and MWPF failed at a load that was twice as high as that of specimen MWN. The two specimens are structurally safe even at 0.4 g, which is the standard seismic acceleration for masonry structures specified in TMS-420 of the U.S. International Building Code [30]. The displacement values of specimen MWPF5 at all loads were higher than those of other specimens; MWPF5 failed at the highest load. In MWPF5, two GFRP strips in diagonally crossing pattern were attached to the wall surface; consequently, cracks that occurred inside the wall were controlled by the adhesion between the wall and GFRP. When debonding occurs between the wall surface and GFRP, the wall is considered to have failed.

3.4. Hysteretic curves and dynamic characteristics

The response of the specimens in terms of hysteretic curves behavior was also evaluated. Figs. 20–22 present the hysteretic curves of each specimen. For each type of specimens, the specimen with complete and uninterrupted data collection is used for drawing hysteresis graph. For non-strengthened, STPU strengthened, and GFRP-STPU strengthened specimens, MWN-3, MWP2-2, and MWPF5-

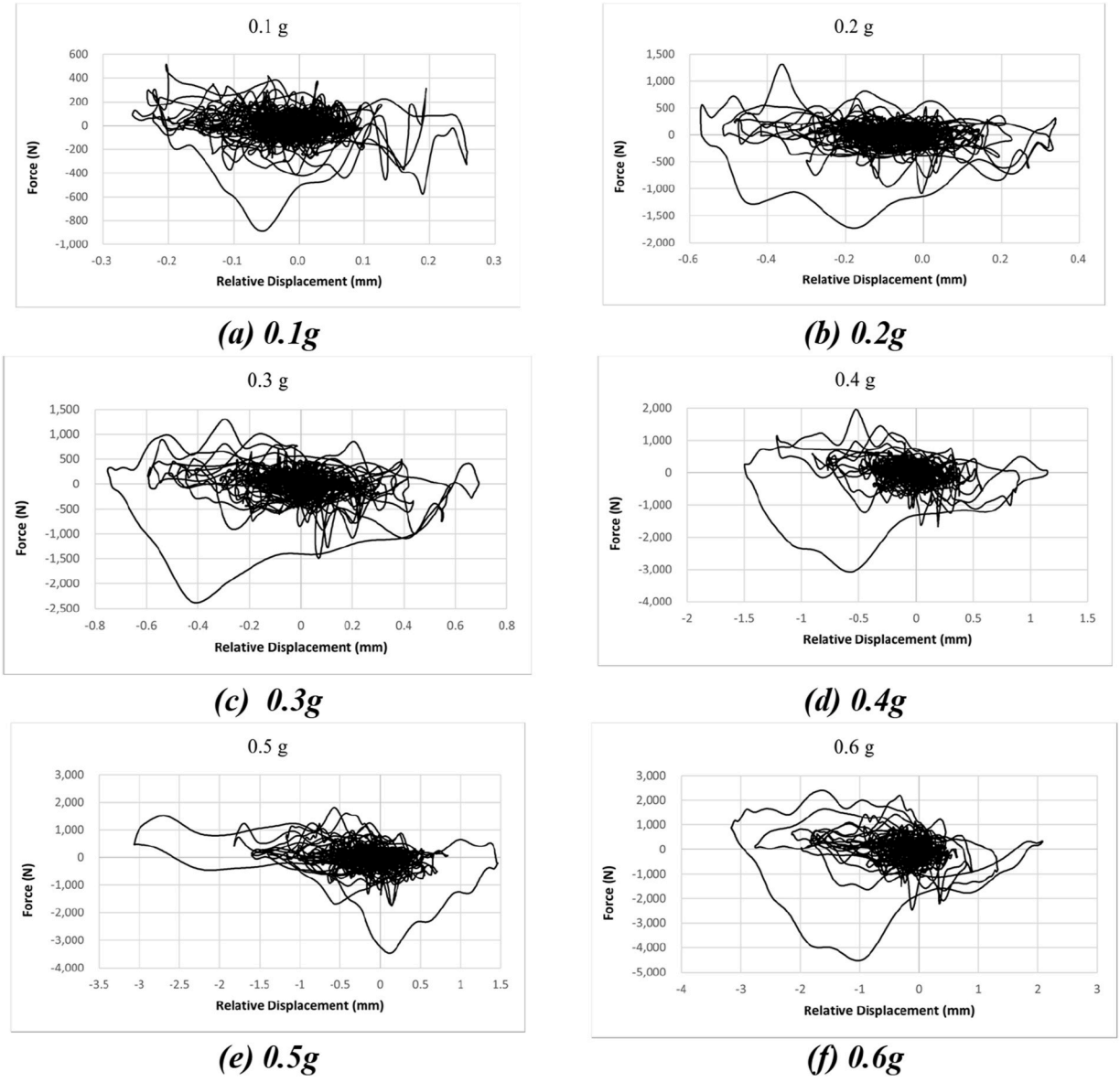

Fig. 21. MWP2-2 specimen hysteretic curves.

2 data were selected for hysteretic curve presentation. The horizontal axis of each graph represents the relative displacement, which is the difference between the displacement of the specimen's top and bottom of the wall. The vertical axis represents the force applied to the specimen, derived from the acceleration data (ABK) recorded during the shaking table test.

Stiffness degradation was assessed by taking the stiffness at 0.1 g as the initial stiffness and comparing it with the stiffness at the peak ground acceleration (PGA) before failure, as summarized in Table 9. The initial stiffness values were highest in the order of MWPF5, MWP2, and MWN. The MWPF5 specimen exhibited an initial stiffness more than twice that of the other two specimens, confirming the effectiveness of GFRP strengthening in enhancing the stiffness of masonry walls. The stiffness degradation ratio was highest in the order of MWPF5, MWP2, and MWN. The significant stiffness degradation observed in MWPF5 is attributed to the debonding of GFRP from the masonry wall due to repeated seismic loading, which considerably reduced the stiffness enhancement effect of the GFRP. The approximately 30 % lower initial stiffness of MWP2 compared to MWN is considered as a variation caused by the non-homogeneous characteristics of the specimen. It is inferred that polyurea is more effective in improving the ductility of the structure rather than stiffness.

The energy dissipation effect of the strengthening materials used in each specimen was evaluated by integrating the area within the envelopes of the hysteresis graphs in Figs. 20–22. The calculated values are summarized in Table 10. A comparison of the energy

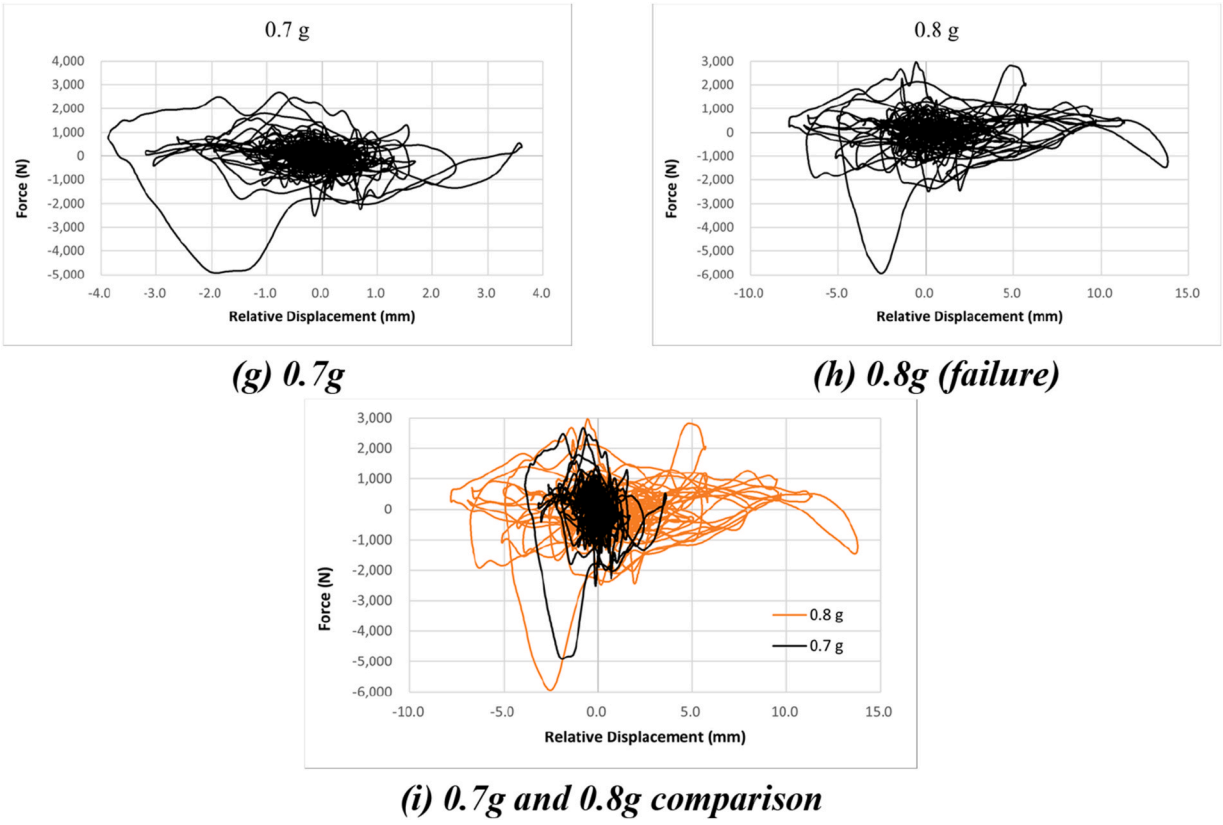

Fig. 21. (*continued*).

dissipation before failure with that of the MWN specimen indicates that the MWP2 and MWPF5 specimens exhibited values that were 5.2 and 10.5 times higher, respectively. This result demonstrates the superior strengthening performance of STPU in resisting dynamic out-of-plan seismic loading.

The damping ratio was calculated using the logarithmic decrement method, as described in Eqs. (1) and (2), based on the free vibration response data recorded after the cessation of seismic excitation.

$$\delta = \ln\left(\frac{X_n}{X_{n+1}}\right) \tag{1}$$

$$\gamma = \frac{\delta}{\sqrt{4\pi^2 + \delta^2}} \tag{2}$$

where X_n is n-th peak amplitude, X_{n+1} is n+1-th peak amplitude; δ is logarithmic decrement; γ is damping ratio.

The damping ratio was categorized into two states: the values measured at PGA of 0.1 g (elastic state) and at failure (failure state), as summarized in Table 11. The increase in the damping ratio was most pronounced in the order of MWPF5, MWN, and MWP2. A significantly higher damping ratio in the failure state compared to the elastic state indicates a greater extent of structural damage. Consequently, the rate of change in the damping ratio for the brittle-failure of MWPF5 and MWN specimens was 2.81 and 1.59 times higher, respectively, than that of the ductile-failure of MWP2 specimen.

4. Conclusions

STPU is developed by modifying the components of existing PU to achieve a better strengthening effect. In this study, the strengthening effect of STPU for masonry wall structures was evaluated. The extreme condition of the shaking table tests was investigated for three types of specimens, and the displacement and acceleration of each specimen were measured. The test results are summarized as follows.

1) Regarding the average experimental values between specimens MWN and MWP2, failure occurred when the seismic loads were 0.4g–0.5 g and 0.7g–0.8 g, respectively. Thus, the seismic load resistance of specimen MWP2 was 0.2g–0.4 g higher than that of

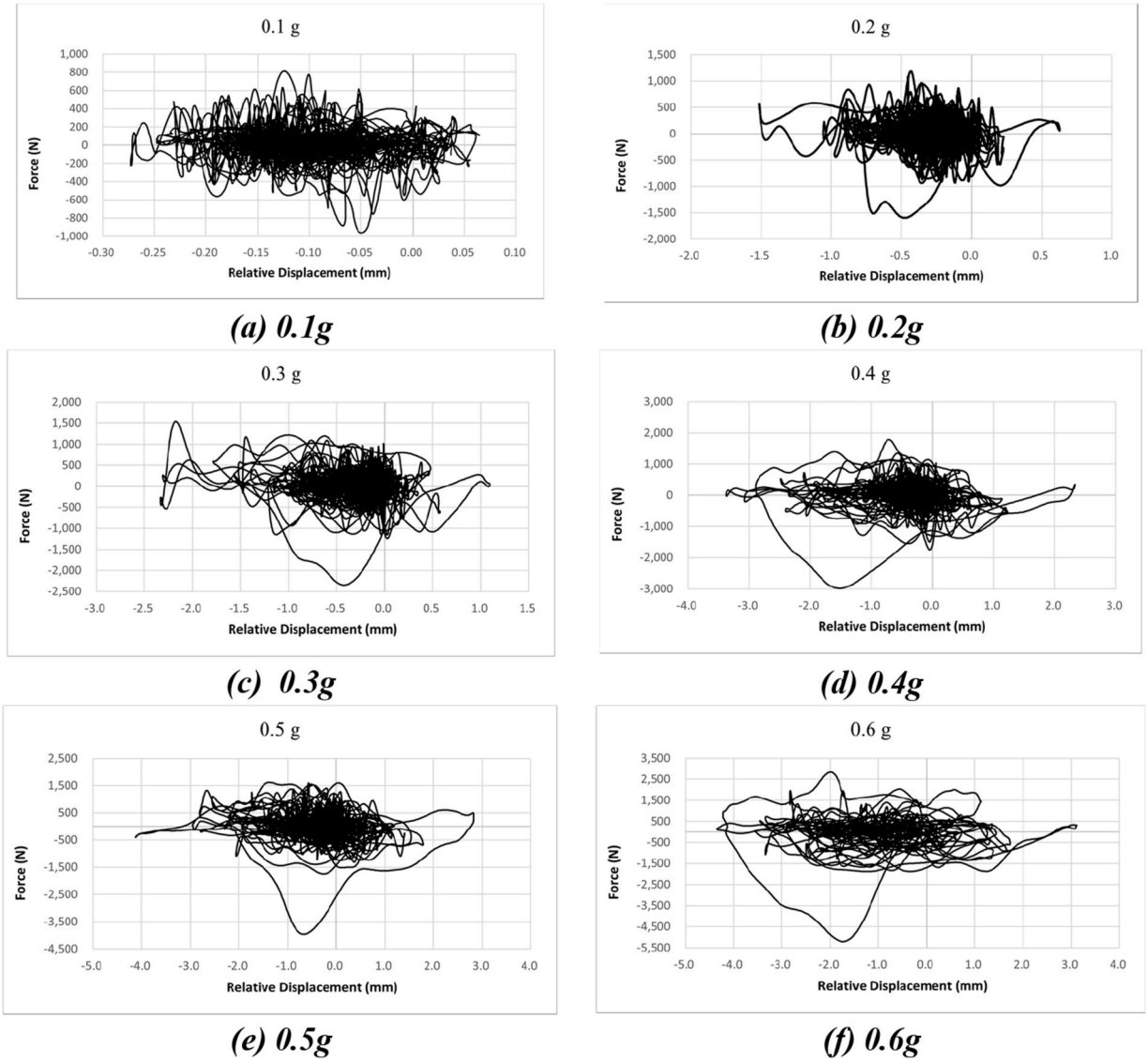

Fig. 22. MWPF5-2 specimen hysteretic curves.

specimen MWN. Strengthening with STPU increased the ductility of the structure, resulting in higher seismic load resistance. As ductility increased, an increase in energy absorption and a reduction in structural acceleration were observed.

2) Based on relative displacement, both specimens MWP2 and MWPF failed at a load that was twice as high as that of specimen MWN. The two specimens are structurally safe even at 0.4 g, which is the standard seismic acceleration for masonry structures specified in TMS-420 of the U.S. International Building Code [30].
3) The displacement values of specimen MWPF5 at all loads were higher than those of other specimens; MWPF5 failed at the highest load. In MWPF5, two GFRP strips were attached to the wall surface in diagonally crossing patter; consequently, cracks that occur inside the wall are controlled by the adhesion between the wall and GFRP. When debonding occurs between the wall surface and GFRP, the wall is considered to have failed.
4) The shaking table test results revealed that the hybrid STPU-GFRP strengthened wall exhibited the highest seismic load resistance among the three types of specimens. More specifically, MWPF5 specimen withstood seismic loads up to 0.9 g–1.0 g, which is 0.1 g–0.3 g higher than MWP2 and 0.4 g–0.6 g higher than MWN. Due to the higher stiffness of GFRP compared to STPU, the hybrid GFRP-STPU strengthening method exhibited a greater confinement effect, leading to increased seismic resistance. However, the specimens strengthened with GFRP-STPU showed a higher acceleration response under seismic loading due to the increased stiffness, indicating a potential risk of brittle failure upon collapse.

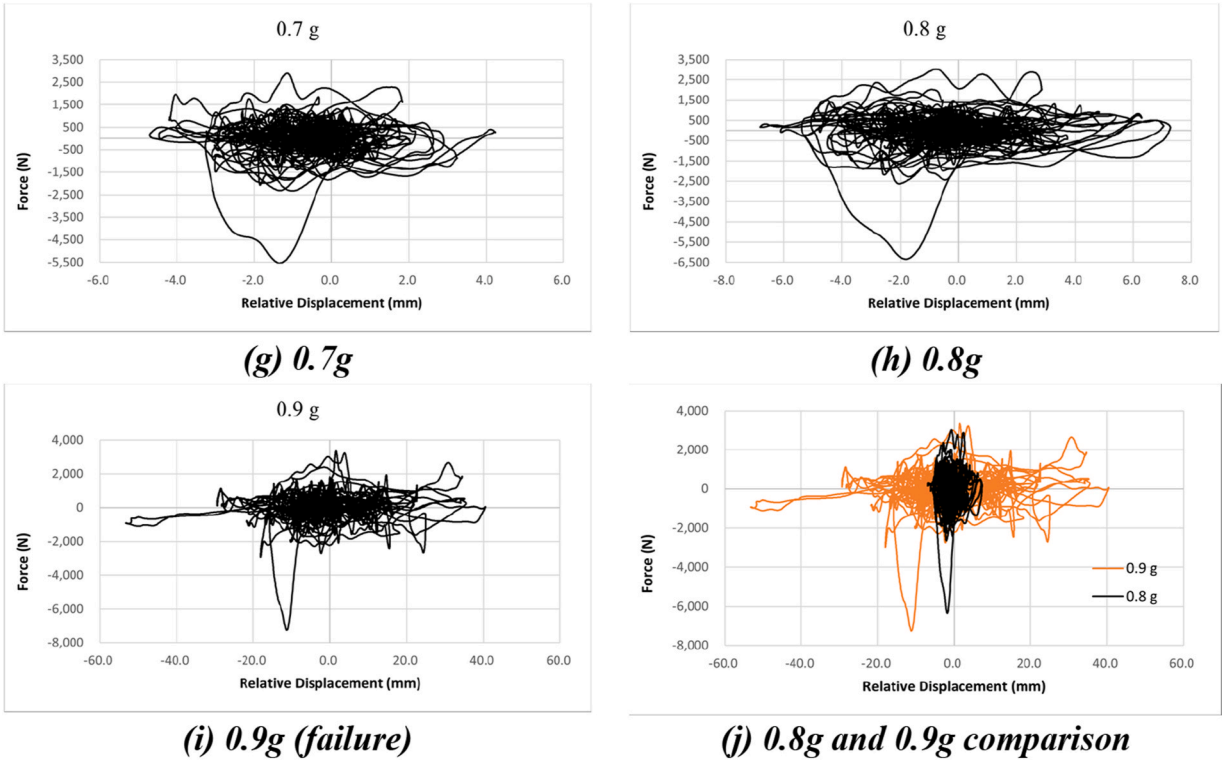

Fig. 22. (*continued*).

Table 9
Stiffness degradation [unit: MPa].

Specimen	Initial stiffness (*I*)	Stiffness before failure (*E*)	Degradation ratio
MWN-3	9.76	5.26	0.46
MWP2-2	6.86	2.56	0.63
MWPF5-2	19.60	3.52	0.82

*Degradation ratio: $\frac{I-E}{I}$

Table 10
Energy dissipation comparison among three types of specimens [unit: joule(J)].

PGA	Spcm.		
	MWN-3	MWP2-2	MWPF5-2
0.1 g	0.21	0.16	0.14
0.2 g	1.25	0.68	1.27
0.3 g	2.56	1.32	2.86
0.4 g	48.6 (failure)	2.87	5.80
0.5 g	–	4.72	7.50
0.6 g	–	9.07	12.72
0.7 g	–	13.32	15.34
0.8 g	–	32.62 (failure)	26.88
0.9 g	–	–	119.52 (failure)

Table 11
Damping ratio according to specimen condition.

Specimen	Damping ratio (elastic state (E))	Damping ratio (failure state (F))	Ratio (F/E)
MWN-3	5.21 %	13.50 %	2.59
MWP2-2	6.97 %	11.33 %	1.63
MWPF5-2	4.85 %	22.28 %	4.59

5) The experimental results demonstrated that GFRP-STPU strengthening significantly improved the initial stiffness of masonry walls, though stiffness degradation occurred due to GFRP debonding under repeated seismic loading. The damping ratio results indicated that STPU primarily enhances ductility rather than stiffness. These findings suggest that STPU-based retrofitting offers a promising alternative to conventional methods, providing improved energy dissipation and ductility. Further studies on long-term durability and practical applications are recommended.

CRediT authorship contribution statement

Tae-Hee Lee: Writing – review & editing, Writing – original draft, Investigation. **Jang-Ho Jay Kim:** Supervision, Methodology, Conceptualization.

Declaration of competing interest

The authors declare that they have no known competing financial interests or personal relationships that could have appeared to influence the work reported in this paper.

Acknowledgements

This work is supported by the Korea Agency for Infrastructure Technology Advancement (KAIA) grant funded by the Ministry of Land, Infrastructure and Transport (Grant RS-2021-KA163381).

Appendix A. Supplementary data

Supplementary data to this article can be found online at https://doi.org/10.1016/j.jobe.2025.112963.

Data availability

Data will be made available on request.

References

[1] H.W. Nam, The Status of Earthquake Occurrence in Korea in 2013, Press Release of Korea Meteorological Administration, Korea, 2014.
[2] T.K. Hong, S. Park, J. Lee, W. Kim, Spatiotemporal seismicity evolution and seismic hazard potentials in the western East Sea (Sea of Japan), Pure Appl. Geophys. 177 (8) (2020) 3761–3774.
[3] Korea Meteorological Administration (KMA), Earthquake, Korea. https://www.weather.go.kr/plus/eqkvol/domesticlist.jsp?startTm=2016-01-01&endTm=2016-1230&startSize=5.0&endSize=5.5&startLat=&endLat=&startLon=&endLon=&lat=&lon=&dist=&keyword=&schOption=T&x=37&y=7, September, 2016.
[4] C. Kim, The effects of geographical distance, involvement, emotion to earthquake on risk perception, Crisisonomy 13 (5) (2017) 59–73.
[5] D.G. Lee, T.H. Kim, Application of seismic isolation and vibration control in Korea, J. Earthq. Eng. Soc. Korea 10 (6) (2006) 67–77.
[6] Seoul institute of Technology (SIT), spotlight. https://www.sit.re.kr/kr, June, 2020.
[7] M. Bruneau, State-of-the-art report on seismic performance of unreinforced masonry buildings, J. Struct. Eng. 120 (1) (1994) 230–251, https://doi.org/10.1061/(ASCE)0733-9445(1994)120:1(230.
[8] S. Cholostiakow, B. McKinley, P. Mergos, C. Hall, A. Kappos, A. Ayoub, Seismic retrofitting of URM masonry piers with helical steel reinforcement, Constr. Build. Mater. 431 (2024) 136499.
[9] K. Meguro, N. Sathiparan, K. Sakurai, M. Numada, Shaking table test of two-story masonry house model retrofitted by PP-band mesh, in: Proc., 15th World Conf. on Earthquake Engineering (15WCEE), Sociedade Portuguesa de Engenharia Sismica (SPES), 2012. Portugal.
[10] T.A. Mukhamediev, V.R. Falikman, Design of externally bonded FRP systems for strengthening of concrete structures, in: Proceedings of the 4th International Conference on Concrete Repair, Rehabilitation and Retrofitting, 2015 2016, pp. 183–184. ICCRRR.
[11] CNR-DT 200/2004, Guide for design and construction of externally bonded FRP systems for strengthening existing structures. Materials, RC and PC structures, masonry structures. Advisory Committee on Technical Recommendations for Construction, National Research Council, Rome, 2004.
[12] L.C. Hollaway, J.G. Teng (Eds.), Strengthening and Rehabilitation of Civil Infrastructures Using Fibre-Reinforced Polymer (FRP) Composites, Elsevier, 2008.
[13] G. Nilakantan, R.L. Merrill, M. Keefe, J.W. Gillespie Jr, E.D. Wetzel, Experimental investigation of the role of frictional yarn pull-out and windowing on the probabilistic impact response of Kevlar fabrics, Compos. B Eng. 68 (2015) 215–229.
[14] N. Maerz, A. Nanni, J. Myers, G. Galecki, Laser profilometry for concrete substrate characterization prior to FRP laminate application, Concr. Repair Bulletin 14 (3) (2001) 4–8.
[15] G. Milani, E. Grande, E. Bertolesi, T. Rotunno, M. Fagone, Debonding mechanism of FRP strengthened flat surfaces: analytical approach and closed form solution, Constr. Build. Mater. 302 (2021) 124144.

[16] X. Min, J. Zhang, X. Li, C. Wang, Y. Tu, G. Sas, L. Elfgren, A nonlinear prediction model of the debonding process of an FRP-concrete interface under fatigue loading, Constr. Build. Mater. 369 (2023) 130583.
[17] M. hossein Saghafi, H. Shariatmadar, Enhancement of seismic performance of beam-column joint connections using high performance fiber reinforced cementitious composites, Constr. Build. Mater. 180 (2018) 665–668.
[18] M. Mercuri, M. Vailati, A. Gregori, Two-heads brick masonry walls strengthened by basalt and glass chopped fiber mortar: effect of bed joints and coating reinforcements, Structures 64 (2024) 106530.
[19] G. Arslan, F. Sevuk, I. Ekiz, Steel plate contribution to load-carrying capacity of retrofitted RC beams, Constr. Build. Mater. 22 (3) (2008) 143–153.
[20] D.R. Sahoo, D.C. Rai, Seismic strengthening of non-ductile reinforced concrete frames using aluminum shear links as energy-dissipation devices, Eng. Struct. 32 (11) (2010) 3548–3557.
[21] G. Papavasileiou, N. Pnevmatikos, The cost of retrofitting steel-concrete composite buildings against progressive collapse with steel cables, Int. J. Prog. Sci. Technol. (IJPSAT) 6 (1) (2017) 103–115.
[22] J. He, X. Sun, D. Pi, X. Wang, M. Wu, W. Qin, A. Wu, Y. Qu, B. Wang, An experimental study on the resistance of a polyurea-sprayed structure to low-speed drop hammer impact, Constr. Build. Mater. 435 (2024) 136915.
[23] S. Parniani, H. Toutanji, Monotonic and fatigue performance of RC beams strengthened with a polyurea coating system, Constr. Build. Mater. 101 (2015) 22–29.
[24] J.S. Davidson, J.R. Porter, R.J. Dinan, M.I. Hammons, J.D. Connell, Explosive testing of polymer retrofit masonry walls, J. Perform. Constr. Facil. 18 (2) (2004) 100–106.
[25] H. Guo, C. Du, Y. Chen, D. Li, W. Hu, X. Lv, Study on protective performance of impact-resistant polyurea and its coated concrete under impact loading, Constr. Build. Mater. 340 (2022) 127749.
[26] W.B. Huang, J.Y. Xiang, P. Lv, X.M. Li, Study on mechanical properties aging of spray pure polyurea for hydraulic concrete protection, in: Advanced Materials Research, 374, Trans Tech Publications, 2012, pp. 1325–1329.
[27] D. Chen, H. Wu, Q. Fang, J.S. Wei, S.L. Xu, Out-of-plane behaviors of unreinforced and spray polyurea retrofitted one-way masonry infilled walls, J. Build. Eng. 67 (2023) 106006.
[28] T.H. Lee, J.H. Park, D.H. Yang, J.H.J. Kim, N.B.M. Noor, Material enhancements of newly developed stiff type polyurea for retrofitting of concrete structures, Case Stud. Constr. Mater. 17 (2022) e01431.
[29] N.M.K. Lamba, K.A. Woodhouse, S.L. Cooper, Polyurethanes in Biomedical Applications, first ed., CRC PRESS, United States of America, 1998, pp. 14–23.
[30] Building code requirements and specification for masonry structures: containing building code requirements for masonry structures, TMS 402-08/ACI 530-08/ASCE 5-08), Specification for Masonry Structures (TMS 602-08/ACI 530.1-08/ASCE 6-08) and Companion Commentaries, Masonry Society, 2008.